# Quantum cascade lasers operating from 1.2 to 1.6 THz

Christoph Walther,[a] Milan Fischer, Giacomo Scalari, Romain Terazzi, Nicolas Hoyler, and Jérôme Faist[b]
*Institute of Physics, University of Neuchâtel, CH-2000 Neuchâtel, Switzerland*

(Received 28 June 2007; accepted 11 September 2007; published online 28 September 2007)

Two terahertz quantum cascade lasers based on GaAs/$Al_{0.1}Ga_{0.9}As$ heterostructures are reported. Pulsed mode operation up to 84 K and continuous wave (cw) power of 0.36 mW at 10 K are demonstrated for the laser which emits from 1.34 to 1.58 THz. The other laser shows emission from 1.2 to 1.32 THz with pulsed mode operation up to 69 K and cw power of 0.12 mW at 10 K.
 [DOI: 10.1063/1.2793177]

Since the demonstration of the terahertz quantum cascade laser[1] (QCL) much progress has been made. Output powers up to 248 mW in the pulsed mode with 138 mW in the cw mode and a highest pulsed mode operating temperature of 164 K have been demonstrated in the frequency range from 3 to 4.4 THz.[2,3] The operation range of terahertz QCL spans from 4.8 (Ref. 4) to 1.6 THz (Ref. 5) and down to 1.39 THz using strong magnetic fields.[6] Although the air is opaque in the terahertz range due to strong water absorption lines, there are transmission windows especially at low frequencies, 1.5, 1.3, 1 THz, and below (calculated from the HITRAN database), which are technologically interesting for applications such as imaging.[7]

Two major challenges have to be faced in order to extend terahertz QCLs to lower frequencies. Between two closely lying subbands ($\Delta E < 6$ meV) a population inversion has to be achieved which requires a high injection selectivity of carriers in the upper state and lifetime engineering based on the dominant scattering mechanisms. Second, a low loss waveguide has to be realized despite the $\lambda^2$ wavelength dependence of the free-carrier absorption.[8]

In this paper we demonstrate two terahertz QCLs, which cover the frequency range from 1.2 to 1.6 THz, corresponding to an optical transition between subbands spaced by only 5–6.6 meV.

LO-phonon scattering between subbands spaced by a few meV is not allowed at low temperature. The dominant scattering mechanism in the absence of LO-phonon scattering was believed to be electron-electron (*e-e*) scattering.[9,10] The consequence of the low energy spacing $\Delta E$ between the subbands in the active region would result in a strong decrease of the upper state lifetime due to the $1/\Delta E$ dependence of the *e-e* scattering rate and increase the difficulty to obtain a sufficiently high population inversion.[11]

The study of Kempa *et al.* of a quantum cascade structure in a strong magnetic field points out the relative weight of *e-e* and elastic single-electron scattering, coming to the conclusion that the latter is about ten times stronger than *e-e* scattering.[12] Single-electron scattering includes interface roughness (IR) scattering, alloy disorder scattering, and ionized impurity (*e*-imp) scattering. Recent results show strong evidence that IR scattering is dominant if LO-phonon scattering is suppressed or inefficient.[13,14]

Figure 1(a) shows the band structure of sample N892, which is based on a bound-to-continuum transition with an energy gap that separates the miniband from the two injector states.[5] The second sample, labeled N908, has an almost identical band structure. The advantage of the bound-to-continuum scheme[15] is the large phase space for scattering out of the upper and lower states. By considering only IR scattering, a population inversion between states 8 and 6 is predicted at low temperature. Using the formalism of Ref. 16 and phenomenological parameters $\Delta = 0.4$ nm and $\Lambda = 7.5$ nm, for both samples typical values of $\tau_8$, $\tau_6 \sim 10$ ps, and $\tau_{86} \sim 20-30$ ps are calculated during the injection regime ($T = 0$ K). The qualitative prediction for a population inversion, $\tau_6/\tau_{86} < 1$, is independent of the precise phenomenological parameters. Although IR scattering may be the dominant diffusion mechanism of the upper state,

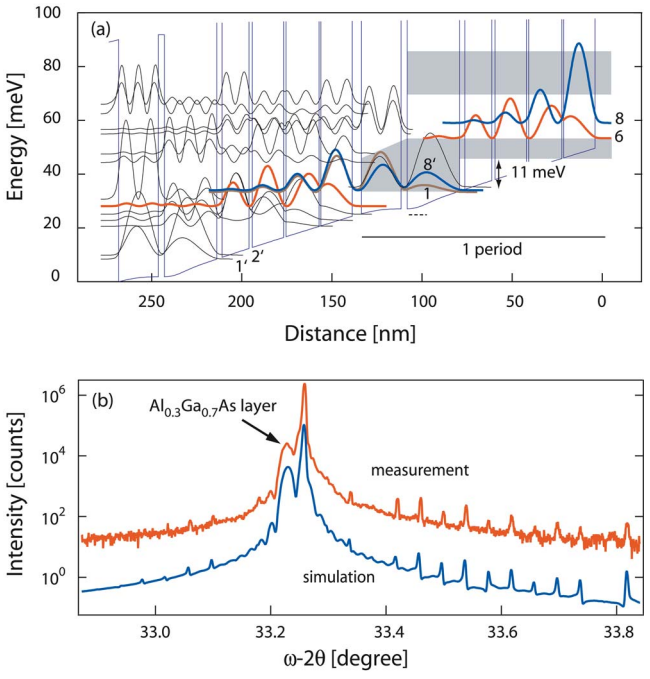


FIG. 1. (Color online) (a) Self-consistent solution ($T = 50$ K) of coupled Schrödinger and Poisson equations for an applied electric field of 1.95 kV/cm for N892. The nominal layer sequence, starting from the injection barrier is (in nm): **5.1**/17.4/**1.0**/18.4/**1.3**/17.4/**1.8**/14.9/**2.9**/19.2/10.0/**3.3**/22.0. $Al_{0.1}Ga_{0.9}As$ barriers are represented by bold face numbers and the underlined layer is doped with Si, $2.7 \times 10^{16}$ cm$^{-3}$ in density. The doping level yields a nominal sheet carrier density of $2.7 \times 10^{10}$ cm$^{-2}$ and an average doping density of $2 \times 10^{15}$ cm$^{-3}$. (b) Measured and simulated x-ray diffraction of the grown structure (N892).

[a]Electronic mail: christoph.walther@unine.ch
[b]Electronic mail: jerome.faist@unine.ch

 

other scattering mechanisms such as *e*-*e* and *e*-imp scatterings are supposed to contribute significantly to the extraction of electrons from the lower state, which is part of the miniband, leading to a larger predicted population inversion. The energy gap, which is larger than the photon energy, separates the electrons in the injector from the miniband, therefore reducing the possibility of backfilling and of resonant intersubband absorption. The two injector states are off-resonance prior to the alignment with the upper state, which reduces efficiently the parasitic current from the injector in the miniband. At injection resonance with the upper state, the injector states themselves are also in resonance, leading to a high injection efficiency in the upper state.

Low waveguide losses and high confinement factor are obtained with the double metal waveguide.[17] The calculated losses of 19 $cm^{-1}$ for N892 and 19.7 $cm^{-1}$ for N908 are of the same magnitude as the losses in Ref. 5, demonstrating constant waveguide losses in the range from 1.2 to 1.8 THz. The losses of the double metal waveguide are calculated by $\alpha_w = \alpha_m + \alpha_{act}$, where $\alpha_m$ are the losses in the gold contacts and doped contact layers, and $\alpha_{act}$ the losses in the active region. $\alpha_m$ is calculated with a Drude model, which uses the measured values in Ref. 18 for the $n$ and $k$ parameters of the gold contacts. For N892 and N908 losses of 10.3 and 9.5 $cm^{-1}$ are obtained, respectively, showing no significant $\lambda$ dependence. Although free-carrier absorption losses in the doped contact layers are higher at lower frequency, the losses in the gold contacts decrease due to the better conductivity.

The losses in the active region are calculated by taking into account the confinement of the electrons in the growth direction in contrast with the usual model,[19] which treats the active region as bulk with an average doping and which predicts a strong increase of the losses below 2 THz due to the $\lambda^2$ dependence of the free-carrier absorption. In our model the losses in the active region are due to the intersubband absorption, calculated as described in Ref. 5, leading to 8.7 $cm^{-1}$ for N892 and 10.2 $cm^{-1}$ for N908. Band structure engineering allows one to transfer the oscillator strength of the injector absorption on energies above the photon energy by means of the energy gap.

Both structures, N892 and N908, were grown in the same run by molecular beam epitaxy on GaAs substrates. The growth begins with a 300 nm thick $Al_{0.3}Ga_{0.7}As$ etch stop layer, followed by a 500 nm thick bottom contact layer (Si-doped, $n=2\times10^{18}$ $cm^{-3}$), then 85 repetitions of the active region are deposited, and finished by a top contact (Si-doped, 20 nm with $n=2\times10^{18}$ $cm^{-3}$ and 40 nm with $n=5\times10^{18}$ $cm^{-3}$). The grown structures have been verified by x-ray measurements. The relative variations of the thickness are −0.3% for N892 and −0.9% for N908. Figure 1(b) shows the excellent agreement between the measured and simulated x-ray diffraction of the grown structure N892. Samples were processed in a double metal waveguide with nonalloyed Ti/Au contacts, as described in Ref. 5, then cleaved, indium soldered on copper mounts, and measured on the cold finger of a helium flow cryostat.

Samples from the structure N892 are lasing from 1.34 THz ($\lambda=224$ $\mu$m) to 1.58 THz ($\lambda=190$ $\mu$m) and samples from the structure N908 are lasing from 1.2 THz ($\lambda=250$ $\mu$m) to 1.32 THz ($\lambda=227$ $\mu$m). Together these two structures cover the frequency range from 1.2 to 1.6 THz, extending considerably the lowest reported operation frequency of terahertz QCL's.

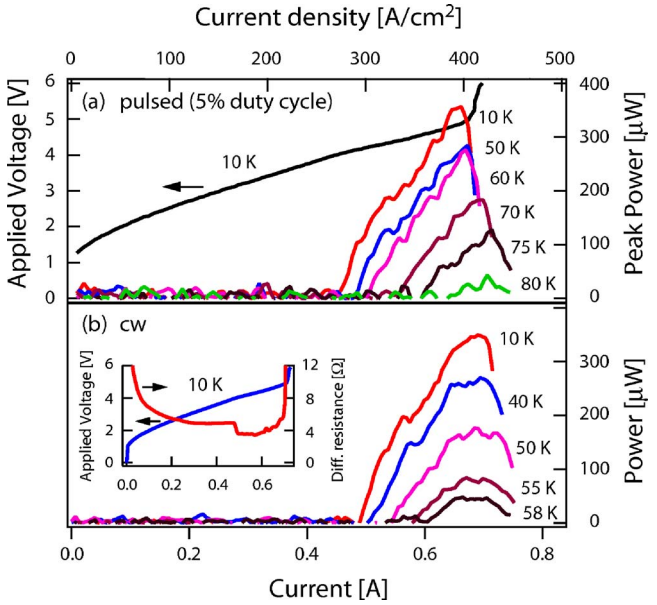


FIG. 2. (Color online) (a) Pulsed and (b) cw *L-I* characteristics of a 1 mm long and 165 $\mu$m wide sample of the structure N892. The inset shows the voltage-current characteristic and differential resistance at 10 K. For the power measurement an absolute terahertz power meter was used (Thomas Keating Instruments). In pulsed mode operation the device was biased with pulse trains of 500 ns repeated at 200 kHz, modulated by a 30.3 Hz square wave, giving an effective duty cycle of 5%. For cw measurements a mechanical chopper at 30.3 Hz was used. The light is collected and guided to the power meter with a straight cone.

Figure 2 shows the *L-I* characteristics of a sample of structure N892. At 10 K the cw threshold current density is 286 $A/cm^2$ and the maximal cw power is 0.36 mW. Operation is observed up to 58 K in the cw mode and up to 80 K in the pulsed mode at a duty cycle of 5%. At a duty cycle of 0.12% the sample operates up to 84 K, as shown in Fig. 4(c).

Figure 3 shows the *L-I* characteristics of a sample of structure N908. At 10 K the cw threshold current density is 291 $A/cm^2$ and the maximal cw power is 117 $\mu$W. Opera-

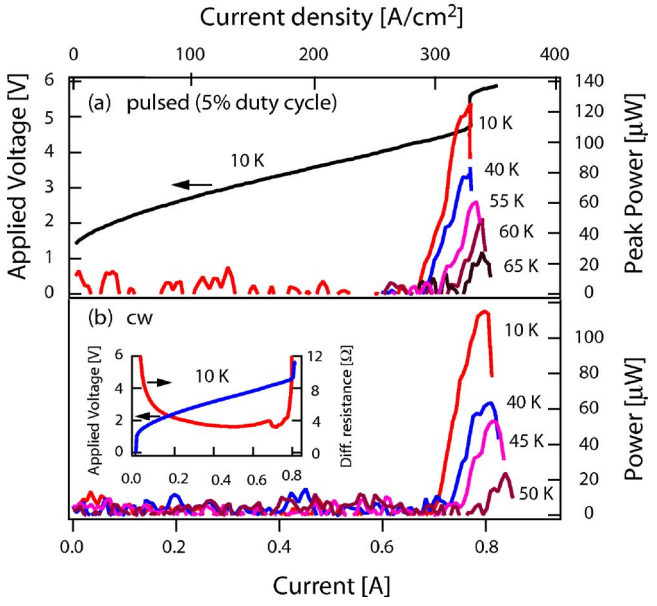


FIG. 3. (Color online) (a) Pulsed and (b) cw *L-I* characteristics of a 1.4 mm long and 165 $\mu$m wide sample of the structure N908. The inset shows the voltage-current characteristic and differential resistance at 10 K. The same power measurement setup as described in the caption of Fig. 2 was used.

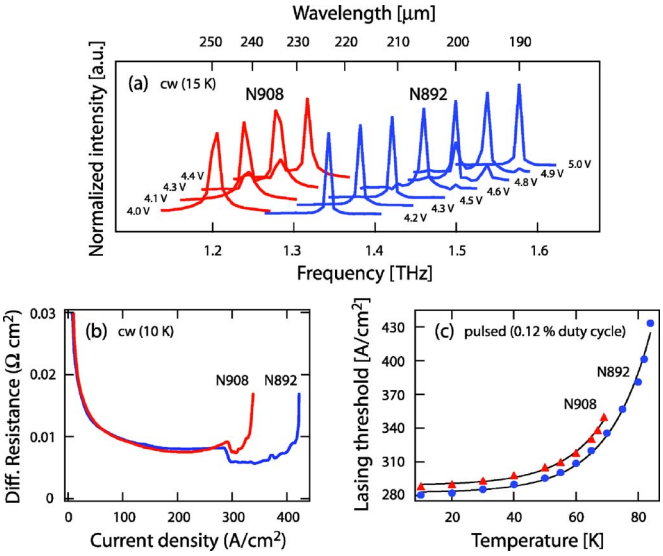


FIG. 4. (Color online) (a) Spectral characterization in the cw mode at 15 K of two devices; one from the structure N892 and the other from N908. Both samples are 1 mm long and 165 $\mu$m wide. (b) Comparison of the differential resistance in the cw mode at 10 K between the devices of Fig. 2 and 3. (c) Threshold current density versus temperature in pulsed mode of the devices of Fig. 2 and 3. The solid lines are guides for the eye. The devices were operated at a very low duty cycle (0.12%) and the lasing threshold was detected with a bolometer.

tion is observed up to 50 K in the cw mode and up to 65 K in the pulsed mode at a duty cycle of 5%. At a duty cycle of 0.12% the sample operates up to 69 K, as shown in Fig. 4(c).

The slope efficiency for the device of the structure N892 of Fig. 2 is 1.7 mW/A, and from Fig. 3 a slope efficiency of 1.24 mW/A is obtained for N908. The relatively low values for the slope efficiency of lasers with a double metal waveguide are related to the large impedance mismatch between the waveguide and the vacuum, which leads to a very high facet reflectivity and a wide angled, patterned far field.[19,20] Using horn antennas the far field can be improved.[21]

cw laser spectra for the two devices are reported in Fig. 4(a) as a function of the applied bias. The spectra were measured with a custom vacuum Fourier transform infrared spectrometer. Both structures show a strong Stark shift of the gain curve with the voltage. Lasing occurs on the Fabry-Pérot modes of the cavity. The strong Stark shift reveals the diagonal nature of the transition and a relatively low ratio of the upper to lower state lifetimes $\tau_{up}/\tau_{dn}$.[22] A large ratio of the lifetimes would lead to a photon controlled transport with pinning of the bias voltage above threshold and no significant Stark shift.[23]

The band structures of N908 and N892 are almost identical. The layer sequence of N908 differs only by a couple of monolayers in the first two quantum wells, which are slightly wider (18.2 and 18.6 nm instead of 17.4 and 18.4 nm), resulting in a lower lying upper state for N908. Compared to N892, the photon energy of N908 is smaller (4.9 meV instead of 5.7 meV) and the dipole is larger (11.3 nm instead of 10.8 nm), resulting in only a slightly lower oscillator strength (16.6 instead of 17.3).

Apart from the lower lasing frequency no significant difference of the laser and transport properties is expected. Under the assumption of identical intersubband scattering times and linewidth of the spontaneous emission, the threshold current density $J_{th}$ reads, $J_{th} \propto \alpha_w/g_c \propto \alpha_w L/f_{86}$, where $\alpha_w$ are the waveguide losses, $f_{86}$ the oscillator strength, and $L$ the length of the period. The calculated ratio of the threshold current densities is $J_{th}^{N892}/J_{th}^{N908}=0.92$, very close to the measured ratio of 0.98. Figure 4(b) shows a comparison of the differential resistance of N892 and N908, clearly showing that the transport prior to the lasing threshold and at the threshold is almost identical. The striking difference of the maximal current density before misalignment is in strong contrast to the identical behavior up to the lasing threshold. The lower maximal current density in the structure N908 is related to the smaller anticrossing gap between the injector state and the upper state at injection resonance.[24] The calculated anticrossing gap $2\hbar\Omega$ for N908 at resonance is 0.54 meV compared to 0.63 meV for N892.

Figure 4(c) shows the threshold current density of both structures as a function of the temperature. The increase of the threshold current density is similar, suggesting that the maximum operating temperature of N908 is not limited by the lower photon energy but by the early misalignment.

This work was supported by Swiss National Science Foundation (NCCR-Quantum Photonics) and EU commission through the IST project "Teranova."

[1] R. Köhler, A. Tredicucci, F. Beltram, H. Beere, E. Linfield, A. Davies, D. Ritchie, R. Iotti, and F. Rossi, Nature (London) **417**, 156 (2002).
[2] B. Williams, S. Kumar, Q. Hu, and J. Reno, Electron. Lett. **42**, 89 (2006).
[3] B. Williams, S. Kumar, Q. Hu, and J. Reno, Opt. Express **13**, 3331 (2005).
[4] A. Tredicucci, L. Mahler, T. Losco, J. Xu, C. Mauro, R. Koehler, H. Beere, D. Ritchie, and E. Linfield, Proc. SPIE **5738**, 146 (2005).
[5] C. Walther, G. Scalari, J. Faist, H. Beere, and D. Ritchie, Appl. Phys. Lett. **89**, 231121 (2006).
[6] G. Scalari, C. Walther, J. Faist, H. Beere, and D. Ritchie, Appl. Phys. Lett. **88**, 141102 (2006).
[7] D. Mittleman, R. Jacobsen, and M. Nuss, IEEE J. Quantum Electron. **2**, 679 (1996).
[8] J. Pankove, *Optical Processes in Semiconductors* (Dover, New York, 1971), pp. 1–422
[9] M. Rochat, J. Faist, M. Beck, U. Oesterle, and M. Ilegems, Appl. Phys. Lett. **73**, 3724 (1998).
[10] J. Smet, C. Fonstad, and Q. Hu, J. Appl. Phys. **79**, 9305 (1996).
[11] P. Hyldgaard and J. Wilkins, Phys. Rev. B **53**, 6889 (1996).
[12] K. Kempa, Y. Zhou, J. Engelbrecht, P. Bakshi, H. Ha, J. Moser, M. Naughton, J. Ulrich, G. Strasser, E. Gornik, and K. Unterrainer, Phys. Rev. Lett. **88**, 226803 (2002).
[13] A. Leuliet, A. Vasanelli, A. Wade, G. Fedorov, D. Smirnov, G. Bastard, and C. Sirtori, Phys. Rev. B **73**, 085311 (2006).
[14] G. Scalari, C. Walther, L. Sirigu, M. L. Sadowski, H. Beere, D. Ritchie, N. Hoyler, M. Giovannini, and J. Faist, Phys. Rev. B **76**, 115305 (2007).
[15] J. Faist, M. Beck, T. Aellen, and E. Gini, Appl. Phys. Lett. **78**, 147 (2001).
[16] T. Unuma, M. Yoshita, T. Noda, H. Sakaki, and H. Akiyama, J. Appl. Phys. **93**, 1586 (2003).
[17] B. Williams, S. Kumar, H. Callebaut, Q. Hu, and J. Reno, Appl. Phys. Lett. **83**, 2124 (2003).
[18] M. Ordal, R. Bell, R. Alexander, L. Long, and M. Querry, Appl. Opt. **26**, 744 (1987).
[19] S. Kohen, B. Williams, and Q. Hu, J. Appl. Phys. **97**, 053106 (2005).
[20] A. Adam, I. Kasalynas, J. Hovenier, T. Klaassen, J. Gao, E. Orlova, B. Williams, S. Kumar, Q. Hu, and J. Reno, Appl. Phys. Lett. **88**, 151105 (2006).
[21] M. Amanti, M. Fischer, C. Walther, G. Scalari, and J. Faist, Electron. Lett. **43**, 573 (2007).
[22] S. Blaser, L. Diehl, M. Beck, J. Faist, U. Oesterle, J. Xu, S. Barbieri, and F. Beltram, IEEE J. Quantum Electron. **37**, 448 (2001).
[23] J. Faist, F. Capasso, C. Sirtori, D. Sivco, A. Hutchinson, and A. Cho, Nature (London) **387**, 777 (1997).
[24] C. Sirtori, F. Capasso, J. Faist, A. Hutchinson, D. Sivco, and A. Cho, IEEE J. Quantum Electron. **34**, 1722 (1998).